

## ARTICLES

# Lack of long-term cortical reorganization after macaque retinal lesions

Stelios M. Smirnakis<sup>1,2</sup>, Alyssa A. Brewer<sup>3</sup>, Michael C. Schmid<sup>1</sup>, Andreas S. Tolias<sup>1</sup>, Almut Schüz<sup>1</sup>, Mark Augath<sup>1</sup>, Werner Inhoffen<sup>4</sup>, Brian A. Wandell<sup>3</sup> & Nikos K. Logothetis<sup>1</sup>

Several aspects of cortical organization are thought to remain plastic into adulthood, allowing cortical sensorimotor maps to be modified continuously by experience. This dynamic nature of cortical circuitry is important for learning, as well as for repair after injury to the nervous system. Electrophysiology studies suggest that adult macaque primary visual cortex (V1) undergoes large-scale reorganization within a few months after retinal lesioning, but this issue has not been conclusively settled. Here we applied the technique of functional magnetic resonance imaging (fMRI) to detect changes in the cortical topography of macaque area V1 after binocular retinal lesions. fMRI allows non-invasive, *in vivo*, long-term monitoring of cortical activity with a wide field of view, sampling signals from multiple neurons per unit cortical area. We show that, in contrast with previous studies, adult macaque V1 does not approach normal responsiveness during 7.5 months of follow-up after retinal lesions, and its topography does not change. Electrophysiology experiments corroborated the fMRI results. This indicates that adult macaque V1 has limited potential for reorganization in the months following retinal injury.

Under many conditions, the brain responds to the loss or distortion of input signals by adjusting the relevant cortical neuronal circuits. Treating dysfunction caused by peripheral damage depends crucially on understanding the nature of this cortical reorganization. Electrophysiological studies indicate that macaque primary visual cortex (V1) might retain a remarkable degree of plasticity into adulthood<sup>1–5</sup>. At 2–6 months after binocular retinal lesions that deprive a zone within V1 of its normal input, stimulus-driven activity is reported to recur up to 5 mm inside the border of the deafferented zone<sup>1,2,4–6</sup> (long-term reorganization). More modest changes in cortical topography spanning 1–2 mm are thought to occur immediately (minutes to hours) after deafferentation<sup>1,7–9</sup> (but see refs 10 and 11).

However, it has not been entirely settled whether significant long-term reorganization occurs in area V1 (refs 12–14). Horton *et al.* find that after monocular retinal lesions in adult macaques, cytochrome oxidase levels in the deafferented V1 zone remain 'severely depressed' for many months, even after enucleation of the remaining eye<sup>13</sup>. Using electrophysiological recordings, Murakami *et al.* found no evidence for topographic reorganization near the deafferented zone induced in macaque V1 by a monocular retinal lesion, although perceptual filling-in clearly occurred at the corresponding visual field scotoma<sup>12</sup>.

To clarify the extent and time course of reorganization in the visual system, we studied signals in macaque V1 after binocular retinal lesions. The lesions were made with a 532-nm photocoagulation laser and were located to create a homonymous visual field scotoma 4–8° in diameter (Fig. 1a–c). These lesions deprived part of V1 of visual input from each eye (cyan region, Fig. 1d), which is thought to be favourable for maximal reorganization<sup>6,8</sup>. We refer to the region in area V1 that is deprived of retinal input as the lesion projection zone (LPZ), following ref. 15.

Using 4.7-T functional magnetic resonance imaging (fMRI) in the anaesthetized macaque<sup>16,17</sup>, we obtained maps of the visually driven

activity in the monkey operculum surrounding the LPZ across time. The activity along the LPZ boundary was monitored every 2–8 weeks, starting 2–3 h after lesioning and continuing for 18–30 weeks. Visually driven activity was assessed by using monocular stimulation to avoid errors associated with potential eye misalignment. We analysed cortical activity along monocular LPZ borders that were also borders for the binocular LPZ (dotted line in Fig. 1d), where reorganization is expected to be maximal<sup>6,8</sup>. We used two visual stimulation paradigms to map cortical activity. In the first stimulation paradigm (full-field) blocks of an 18.4° × 14.1° rotating polar checkerboard pattern alternated with blocks of uniform background illumination. This stimulus strongly and reliably activates early visual areas<sup>16,18</sup>. In the second stimulation paradigm (expanding rings), dynamic annular patterns slowly expanded from fovea to periphery in order to assess the visual field eccentricity maps<sup>19</sup>. We measured the strength of the visually driven signal using coherence<sup>20</sup>, which is equal to the amplitude of the blood-oxygenation-level-dependent (BOLD) signal modulation at the frequency of stimulus presentation, divided by the square root of the power over a range of nearby frequencies (see Methods). The two visual stimulation paradigms yielded the same result with respect to the extent of reorganization.

## LPZ size measured by fMRI remains constant over time

Figure 2a, b shows a coherence map obtained with the expanding-ring stimulus overlaid on a flattened representation of the right visual cortex of the macaque designated E02. There is a well-circumscribed confluent region of low coherence (green) in the right operculum corresponding to the LPZ. The responses in the LPZ have a coherence of less than 0.4, whereas the coherence in immediately adjacent cortex is substantially higher. This level of coherence therefore served as a natural criterion for defining the border between LPZ and normal cortex. It is about 1 s.d. higher than the noise level of

<sup>1</sup>Max Planck Institute for Biological Cybernetics, Spemannstrasse 38, D-72076 Tübingen, Germany. <sup>2</sup>Department of Neurology, Massachusetts General Hospital, 55 Fruit Street, Boston, Massachusetts 02114, USA. <sup>3</sup>Neuroscience Program and Department of Psychology, Stanford University, Stanford, California 94305, USA. <sup>4</sup>Department of Ophthalmology I, University of Tübingen, Schleierstrasse 12, D-72076 Tübingen, Germany.

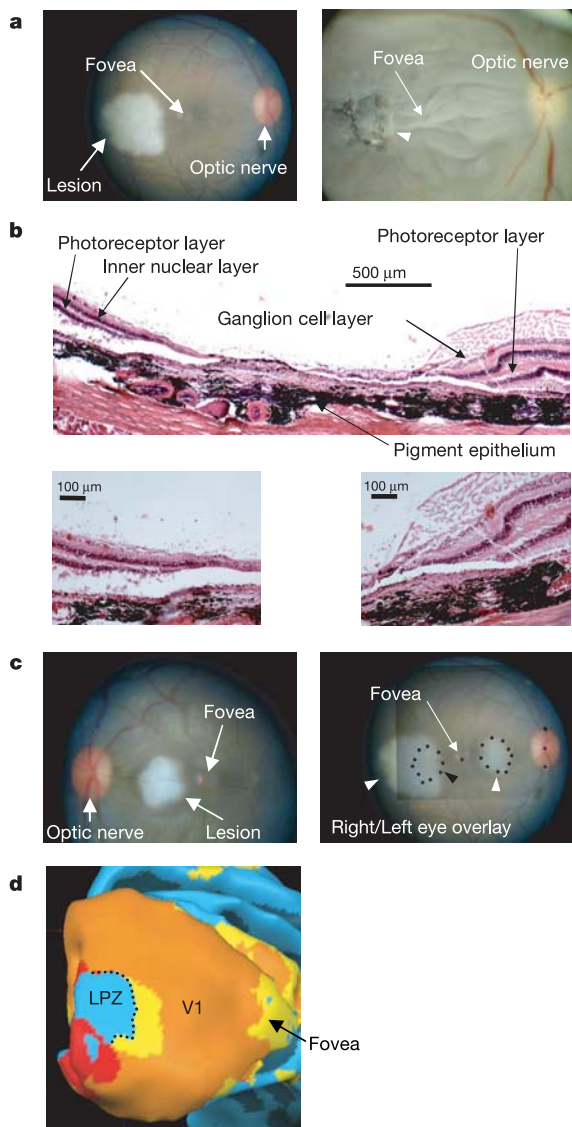


**Figure 1 | Homonymous retinal lesions.** **a**, Left, picture of the right eye fundus 1–2 h after photocoagulation. The lesion appears pale white. Right, right eye cup after extraction and fixation. The lesion (white arrowhead) is scarred and hyperpigmented. Its nasal border is at about  $4^\circ$  eccentricity and the temporal at about  $12^\circ$ . **b**, Top, haematoxylin–eosin stain of a section  $15\ \mu\text{m}$  thick through the right eye lesion in **a**. Note the complete destruction of the photoreceptor layer, as well as the nearly complete obliteration of ganglion and inner nuclear cell layers. Bottom left and right, edges of the haematoxylin–eosin stained section at higher magnification. The photoreceptor layer tapers near the lesion border zone (generally over  $100\text{--}300\ \mu\text{m}$ ). **c**, Left, picture of the left eye fundus 1–2 h after photocoagulation. Right, overlay of the right and left fundi. Lesions are marked by white arrowheads. The left retina (smaller square overlay) was mirrored along the vertical axis and scaled to make the optic nerves overlap. Black dots outline the left eye lesion and its homonymous location in the right eye, which lies almost entirely over the right eye lesion except for a small sliver of normal retina (black arrowhead). This results in a partly homonymous left visual field scotoma. **d**, Eyes were stimulated separately with the full-field checkerboard stimulus (see Methods) and activation maps (voxels with  $P < 0.05$ , uncorrected, cluster criterion 6) were overlaid on the right operculum of monkey O97 by using Brain Voyager (Brain Innovation B.V., Maastricht, The Netherlands). Areas are coloured as follows: yellow, activation through the right eye; red, activation through the left eye; orange, activation map overlap; blue, no visual modulation through either eye. The dotted line marks the segment of the right-eye-LPZ border, where reorganization is expected to be maximal. This is the part of the right-eye-LPZ border that also belongs to the border of the binocular LPZ. The yellow region abutting the LPZ is the projection zone of the sliver of normal retina marked with the black arrowhead in **(c, right)**.

coherence (0.28; see Methods). Using this criterion we outlined the LPZ on a flattened representation of the operculum at various time points: day 0 (black, LPZ<sub>0</sub>), 4 months (cyan, LPZ<sub>4</sub>) and 7.5 months (blue, LPZ<sub>7</sub>) after lesioning (Fig. 2b). There was no significant change in the size of the LPZ over time.

To further ensure that this effect was not an artefact of the particular threshold or the coherence measure itself, we examined the signal modulation both within and adjacent to the LPZ. Figure 2d plots the average signal modulation inside LPZ<sub>0</sub> per stimulation cycle 7.5 months after lesioning; the corresponding plot in Fig. 2g shows the signal modulation derived from an area of approximately the same eccentricity located in normal cortex (see also Fig. 2f, h). We found no significant stimulus-driven modulation inside LPZ<sub>0</sub> even though 7.5 months had passed from the time of the lesion (Fig. 2c–e). Activity inside the V1 lesion projection zone does not return to anywhere near normal levels after homonymous binocular retinal lesions. This result holds true for both stimulation paradigms and for all four macaques used in this study (see also Supplementary Figs 1, 4 and 5). Small, rapid changes that stabilize before the end of the first fMRI session (up to 6 h after lesioning) cannot be excluded.

We also measured the profile of coherence as a function of distance perpendicular to the LPZ border and monitored its changes over time (Fig. 3 and Supplementary Fig. 2). This approach is sensitive and has the advantage that it does not depend on a particular choice of threshold. Using the anatomical scan we selected several thin ( $0.5\text{--}1.0\ \text{mm}$ ) regions of interest (ROIs) parallel to and spanning the BOLD LPZ border (Fig. 3a). The selected ROIs constituted a time-invariant frame of reference based on anatomy, relative to which we could measure changes in the profile of functional activity over time. We then plotted the mean coherence in each ROI as a function of the average distance of the ROI's voxels from the line of zero displacement (represented by the dotted lines in Fig. 3b, c). The line of zero displacement is a line parallel to the LPZ border that serves as the reference point for calculating distances. Although it can be thought of as an estimate of the LPZ border, its position can be chosen arbitrarily because the comparison of coherence profiles across time depends on relative distances only. For clarity we note here that it does not necessarily correspond to the criterion we used to define the LPZ border in Fig. 2b.

The coherence starts high in normal cortex outside the LPZ and decreases gradually to the noise-level coherence deep inside the LPZ, approximating a sigmoidal curve (Fig. 3b). The position and slope of this curve measure the position, the decline in functional activity and the spatial blurring of the signal from normal V1 into the LPZ. Cortical reorganization should be manifested by a shift of the curve towards the interior of the LPZ and/or by a decrease in its slope over time. Electrophysiology literature<sup>1,4,6</sup> suggests that shifts on the order of 5 mm could be expected 2–6 months after lesioning. Given BOLD's sensitivity<sup>17,21,22</sup> and our high ( $1 \times 1\ \text{mm}^2$ ) in-plane functional resolution, we expect to be able to reliably detect border shifts greater than 1 mm, which is half an order of magnitude smaller than shifts reported in the electrophysiology literature<sup>1,4,6</sup>. In Fig. 3b we plot normalized coherence versus distance curves obtained with the full-field stimulus from monkey E02. Different time points are colour coded and overlaid on each other. No shift in position or decline in slope is apparent over the course of 7.5 months. Figure 3c summarizes the results for all monkeys for both retinotopic and full-field stimuli. The LPZ border remains stable to within 1 mm from its original location in all panels, and there is no systematic change in slope (Supplementary Fig. 2). These results remain true for the raw (un-normalized) coherence profiles (Supplementary Fig. 2) and are therefore not an artefact of coherence normalization.

#### Electrophysiological recordings across the LPZ border

A comparison between studies of contrast sensitivity that use the BOLD signal<sup>17,21,22</sup> and electrophysiological recordings<sup>23</sup> indicates that the BOLD signal is sensitive to small increases in multi-unit

activity (smaller than 5% of the response elicited by the high-contrast checkerboard stimulus). However, the BOLD signal also reflects changes in local field potential underlying synaptic activity<sup>17</sup> that can be permanently disrupted inside the LPZ after deafferentiation. We therefore sought to corroborate the fMRI results presented above with electrophysiology experiments.

We performed three multi-electrode electrophysiology experiments after the conclusion of the fMRI sessions. We used a 16-electrode linear array (1-mm spacing) to record across the border of the LPZ (Fig. 4a) in monkey E02. Experimental conditions were identical to those in the fMRI experiments. We manually mapped V1 multi-unit receptive fields for two depths at each electrode location by using small oriented bars and square rotating checkerboard stimuli (Methods). Receptive field maps obtained from the same

electrode at different cortical depths were similar in all cases. Figure 4b illustrates receptive field maps obtained in two such experiments. We mapped receptive fields starting with the electrode closest to the lunate (electrode no. 1) and proceeding towards the border of the LPZ. In all three experiments, our ability to identify multi-unit receptive fields ended at 1.6, 2.2 and 0.8 mm, respectively, outside the LPZ border defined using the fMRI data. We were unable to map classical receptive fields from any electrode located inside the BOLD-defined LPZ border (0/52 recording sites, including depth).

Figure 4c shows firing rate histograms obtained during 10 s of full-field stimulation alternated with 10 s of uniform illumination. During stimulus ON periods, electrode locations outside the LPZ (electrodes 2–10) have steady-state firing rates significantly higher than the spontaneous rates achieved during uniform illumination. In

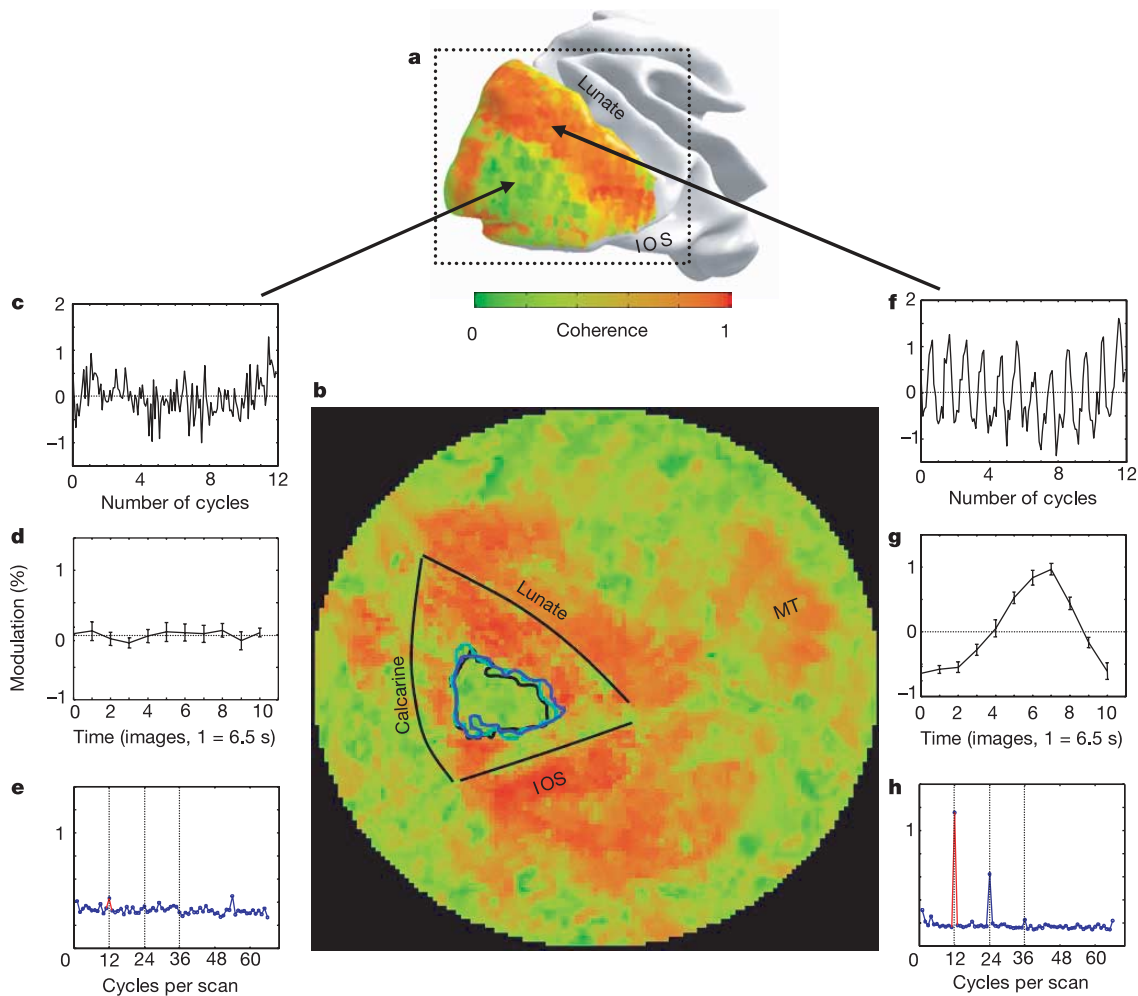


**Figure 2 | BOLD signal inside the LPZ remains at noise level and LPZ size does not change as a function of time after lesioning.** **a**, Coherence map on the right operculum measured with the expanding-ring stimulus (see Methods) presented to the right eye of macaque E02 4 months after lesioning. The green area is the LPZ, a zone of low coherence surrounded by normal cortex. Note that noise level coherence is expected to be 0.28 and not zero (see Methods). **b**, A cortical area of radius 3 cm centred near the fovea was flattened and the coherence map was overlaid. The monkey operculum is outlined by the calcarine, lunate and inferior occipital sulci. Regions of low coherence outside the operculum correspond to non-visual cortex or visual cortex too eccentric to be activated by our stimuli. LPZ borders are shown at 0 days (LPZ<sub>0</sub>, black), 4 months (LPZ<sub>4</sub>, cyan) and 7.5 months (LPZ<sub>7.5</sub>, blue) after lesioning. LPZ size was, respectively, 158, 179 and 180 mm<sup>2</sup> and was larger, if anything, at later time points. Because the LPZ perimeter is about

50 mm this corresponds approximately to an 0.5-mm outward shift of the LPZ border (within noise). A threshold coherence level of 0.4, 1 s.d. above noise level, was used to define the LPZ border at all time points. **c–e**, Signal in LPZ<sub>0</sub> recorded 7.5 months after lesioning. **c**, Percentage modulation of the BOLD signal as a function of stimulus cycles. **d**, Average signal modulation per stimulus cycle (11 rings). **e**, Signal amplitude as a function of temporal frequency. Red marks the frequency of the visual stimulus. Note that the signal amplitude at the stimulus frequency does not differ significantly from the amplitude of noise present at other frequencies ( $P > 0.05$ ). There is therefore no significant stimulus-driven modulation inside the LPZ<sub>0</sub> even 7.5 months after lesioning. **f–h**, Plots corresponding to **c–e** for a region of normal V1 cortex at similar eccentricity to that of the LPZ. Strong visual modulation is evident in all plots. IOS, inferior occipital sulcus; MT, middle temporal area. Error bars represent s.e.m.

contrast, the steady-state firing rates of electrodes inside the LPZ during stimulus ON periods are similar to their firing rates during uniform illumination (Fig. 4c). In Fig. 4d we plot the firing rate modulation strength at steady state during ON/OFF stimulation as a function of distance from the BOLD-defined LPZ border, by pooling and aligning appropriately data from all three experiments. On average, cortical locations inside the LPZ are not significantly modulated by the stimulus at steady state (mean modulation 1.3% with 95% confidence interval  $-2.7$  to  $5.3\%$ ). The border of the LPZ defined by electrophysiology (blue curve) lies about 1 mm outside

the BOLD-defined LPZ border (red curve). The steady-state electrophysiological measurements therefore agree well with the BOLD-defined LPZ border.

The neurons in the LPZ were not entirely silent. There were transient responses at both stimulus onset and offset (Fig. 4c, electrodes 11–16). These transients were insufficient to cause a BOLD response inside the LPZ, probably because they were brief (generally less than 1 s) compared with the 6.0–6.5 s required for the acquisition of one whole-brain image. It is possible that such transients reflect a degree of cortical reorganization, but we do not

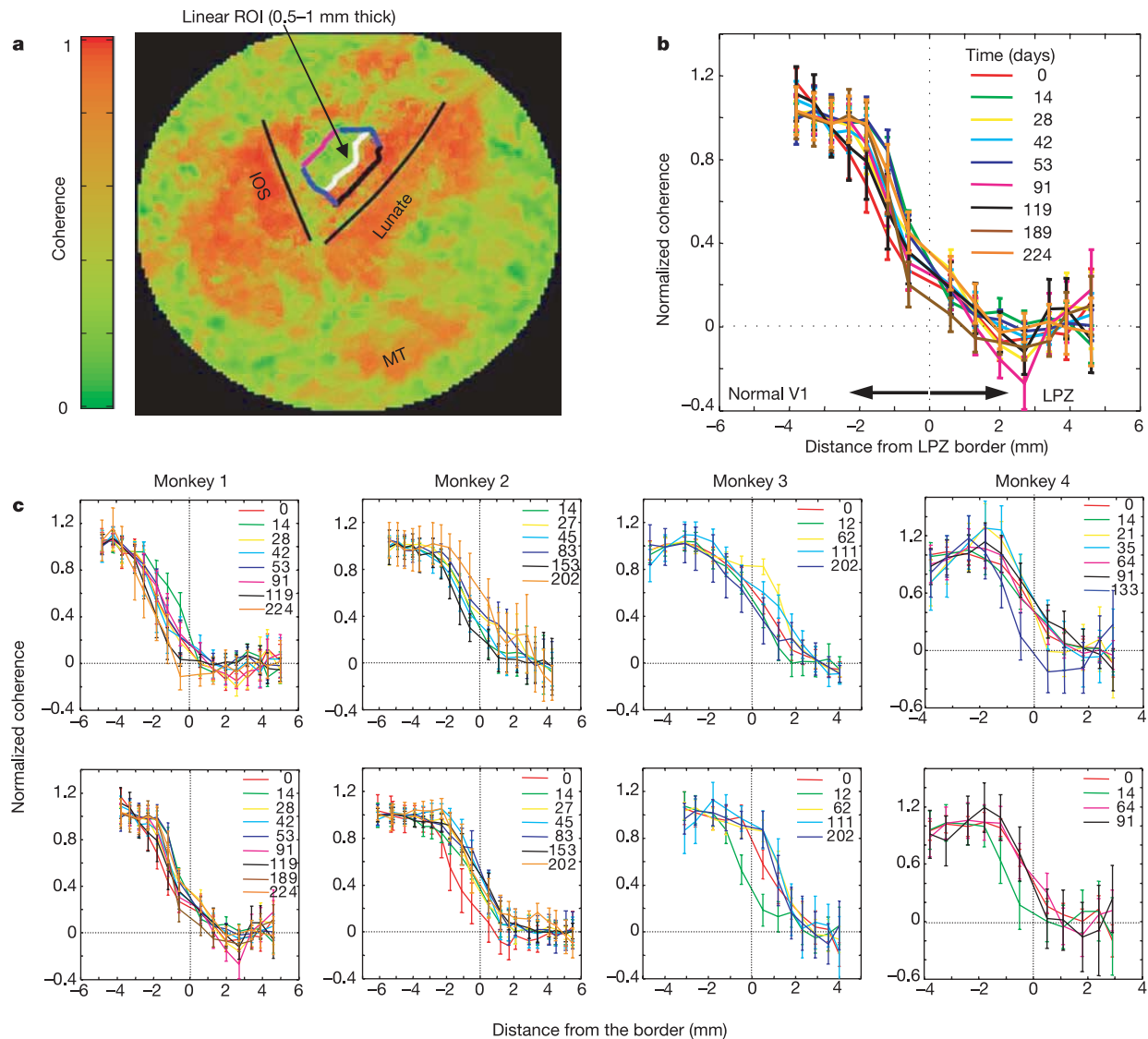


**Figure 3 | The profile of BOLD coherence across the LPZ border does not change as a function of time after lesioning.** **a**, Flattened map of the right operculum of macaque E02 with coherence map overlaid, as in Fig. 2. A set of linear ROIs 0.5–1.0-mm thick, parallel to the LPZ border, was selected to span several millimetres on each side of the border. The white line represents the first ROI located inside the scotoma. The purple line denotes the last ROI selected inside the scotoma, the black line the last ROI selected outside. The blue outline represents the endpoints of all ROIs selected. ROIs are selected once on the anatomical scan and remain the same for all time points. They therefore provide an absolute, time-invariant, reference frame that can be used to gauge whether the profile of functional activity shifts over time. **b**, Monkey E02, full-field stimulation paradigm. The mean coherence of each linear ROI is plotted against the mean distance of that ROI's voxels from the line of zero displacement (represented by the dotted lines at point zero). The resulting sigmoidal curves were normalized to reach a plateau at 0 and 1 by

subtracting the mean of the last four points (that is, noise coherence deep inside the LPZ) and then dividing by the mean of the first four points (that is, the strength of visually driven modulation in normal cortex). Before performing the subtractive normalization we confirmed that the average coherence over the last four points of the sigmoidal curve (which lie inside the LPZ) remained at noise levels throughout. Time is measured in days after lesioning. Different time points are colour coded. Positive distances are towards the LPZ interior, negative towards normal cortex. **c**, Equivalent plots to those in **b** for each monkey (from left to right: E02, A01, O97 and E01). Top row, retinotopic stimulation paradigm; bottom row, full-field stimulation paradigm. Error bars represent s.e.m. There is no consistent shift in position or change in slope of the coherence–distance curve over time (see also Supplementary Fig. 2). The position of the LPZ border is stable to within 1 mm. IOS, inferior occipital sulcus; MT, middle temporal area.

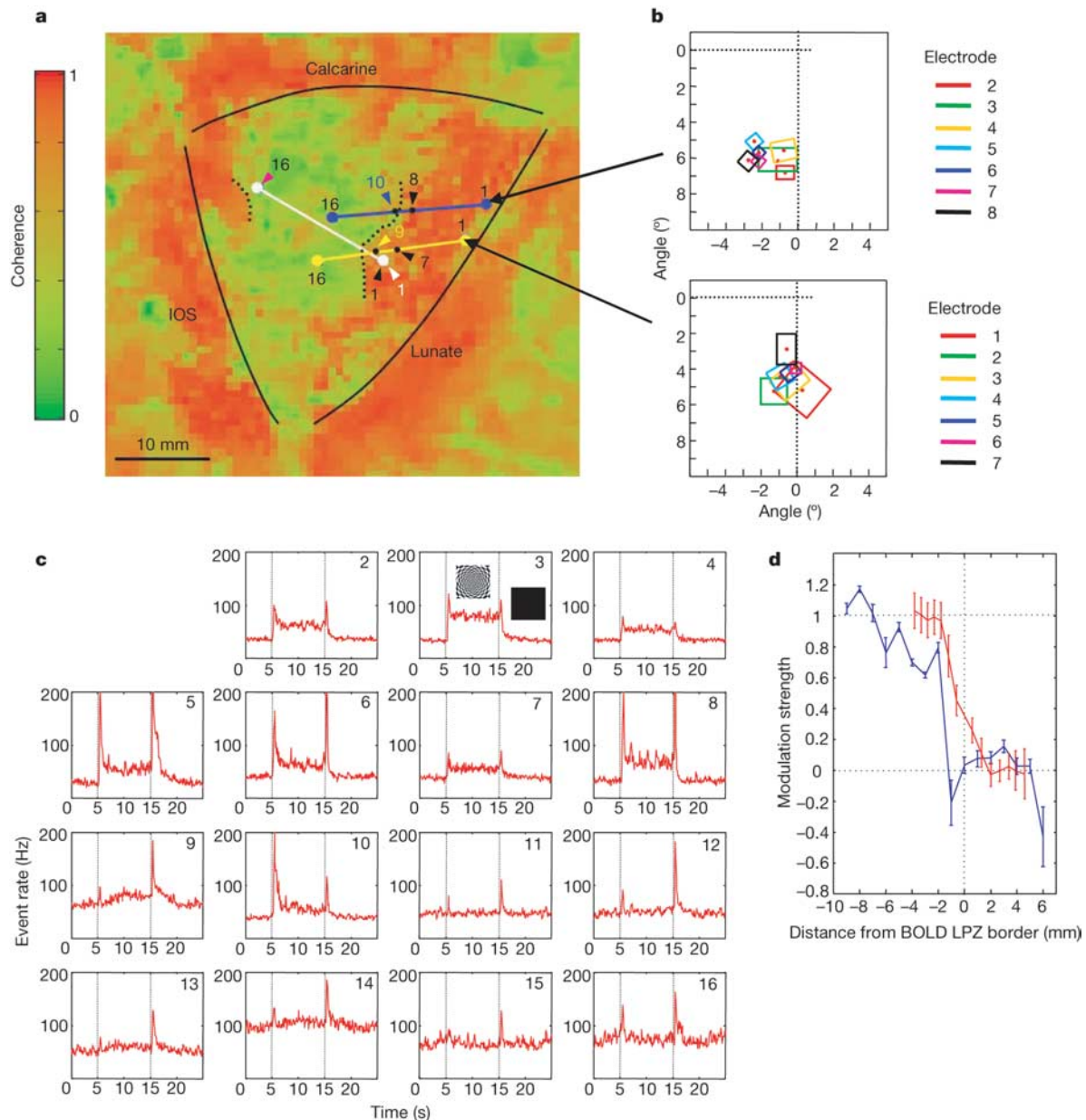


**Figure 4 | Receptive field maps cannot be obtained and steady-state neural responses remain abnormal inside the LPZ.** **a**, Coherence map (day 0, full-field stimulus) overlaid on the flattened right operculum of monkey E02. Each linear trajectory (white, yellow and blue) represents 16 recording electrode locations from one of three experiments. Electrodes were 1 mm apart, starting near the lunate (electrode 1). Black arrowheads mark the last position yielding a multi-unit RF. Blue, yellow and white arrowheads mark the last position whose steady-state multi-unit activity was modulated more than 10% by the full-field stimulus. Dotted lines identify segments of the BOLD-defined LPZ border. The dotted line on the right corresponds to point 0 in Fig. 3b. **b**, Multi-unit RF maps from experiments 2 and 3. RFs could not be mapped with spatially restricted stimuli beyond electrode 1 (experiment 1, data not shown), 7 (experiment 2) and 8 (experiment 3). RF location is accurate to  $1\text{--}2^\circ$  because of slow eye drifts. **c**, Multi-unit firing rate histograms binned at 100 ms for electrodes in experiment 3 (numbers at top right), calculated by averaging 48 cycles of full-field visual stimulation alternating with spatially uniform background intensity (electrode 3 inset). Dotted lines mark stimulus ON (5 s) and OFF (15 s) transitions. Multi-unit activity at steady state is higher during stimulation for electrodes 2–10

(outside the LPZ), but not for electrodes 11–16 (inside the LPZ). Electrode 10 falls on the BOLD-defined LPZ border. Brief ON and OFF firing transients persist inside the LPZ (electrodes 11–16). These may arise through extra-classical receptive field effects known to exist in normal V1 (see Discussion and Supplementary Fig. 3). Transients arising in electrodes with good RF maps (electrodes 2–8) had a mean latency of  $68 \pm 4$  ms compared with  $93 \pm 16$  ms for electrodes near or inside the LPZ border (electrodes 9–16). Electrode 1 was damaged on entry. **d**, Steady-state firing rate (blue) and coherence (red) modulation curves as a function of distance from the BOLD-defined LPZ border. The event-rate modulation strength was calculated as the steady-state (discarding the first 2 s after each transition) firing rate with stimulus ON minus OFF, divided by ON and normalized by dividing by the mean of the first four points, located in normal cortex. Data from all three physiology experiments were used after being aligned appropriately with respect to the LPZ border. Inside the LPZ the average event-rate modulation strength was 1.3%, with 95% confidence limits from  $-2.7$  to 5.3%. The 224th day coherence–distance curve (red) from Fig. 3b is plotted for comparison. Accuracy along the x axis is within 1 mm. Error bars represent s.e.m. IOS, inferior occipital sulcus.

think this is likely because we did not observe these transients inside the LPZ during receptive field mapping with spatially restricted stimuli. This indicates that the transients might arise through the spatial summation of extra-classical receptive field responses<sup>24–27</sup> that are present in normal macaque V1 and can extend over considerable cortical distances<sup>25,28</sup>. Indeed, we observed such transients in animals without retinal lesions by stimulating the extra-classical surround (see Supplementary Fig. 3). It is possible that these transient responses are accentuated to somewhat above their normal level by the downregulation of inhibition that is thought to occur inside the LPZ<sup>29,30</sup>. However, even if some plasticity is mediated through these transient responses, it is clear that V1 cortex has not achieved anything like normal responsivity: receptive field maps cannot be obtained and there is no sustained firing to 3.5-Hz visual modulation inside the LPZ border.

## Discussion

Our results contrast with studies<sup>1,3,4,6,31</sup> indicating that substantial long-term reorganization occurs over 2–6 months and that the LPZ border shifts by about 5 mm (refs 1,4). There could be several reasons for this discrepancy. First, long-term reorganization might be restricted to a subset of few sparsely distributed single neurons that form the basis of the physiology experiments. The BOLD response reflects the average activation of ensembles of cells and thus might provide a more complete assessment of overall neuronal recovery. It is also less prone to possible selection bias, which might be a consideration for physiology experiments. Second, changes in the apparent size of the LPZ might occur without reorganization because of retinal recovery from the swelling caused by photocoagulation<sup>13</sup>. Most studies of long-term reorganization are susceptible to this effect because they compare cortical activity immediately after retinal photocoagulation with activity seen several months later<sup>1,3,4</sup>. The

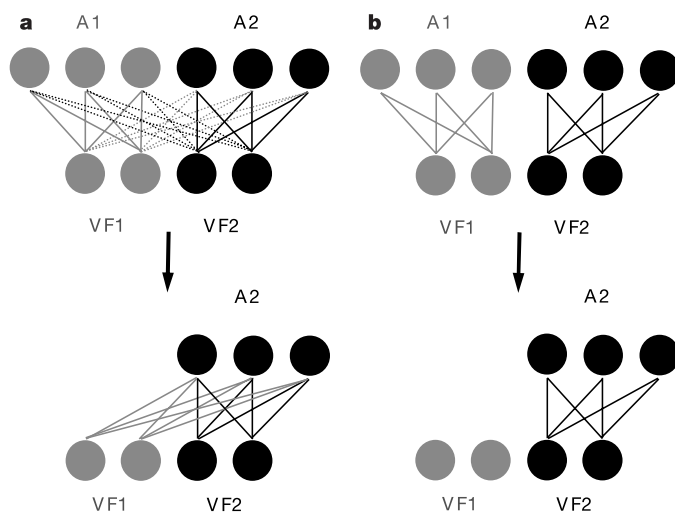


**Figure 5 | Examples of connectivity diagrams.** **a**, The top layer of nodes is the union of two subregions A1 (grey) and A2 (black) with overlapping receptive fields but with connections that have different strengths (dotted, weak; solid, strong) so that A1 processes primarily input in the VF1 sector of the visual field and A2 in the VF2 sector. Although injury to area A1 will create an immediate processing deficit in sector VF1, over time the existing weak connections from A2 to VF1 (dotted grey lines) may strengthen (bottom, solid grey lines) and compensate. This is akin to the robustness seen in densely connected neural networks that have a portion of their nodes damaged. **b**, Such a scheme is not possible if the connectivity pattern is restricted and cells have non-overlapping receptive fields. For area A2 to assume processing in sector VF1, new connections have to form *de novo*, and this may be difficult in the adult central nervous system. Pharmacological manipulations to enhance this process hold great promise for enhancing plasticity in the central nervous system in the future.

width of the LPZ border as judged by the sloping segment of the sigmoidal plots presented in Fig. 3 is about 3–4 mm, corresponding to 1–2° of visual angle or a retinal distance of 150–300  $\mu\text{m}$ . This is similar in extent to the partial damage to the photoreceptor layer seen at the edge of the lesion (Fig. 1b). Recovery of this area, which might be ‘stunned’ immediately after photocoagulation, could lead to apparent activity shifts of 3–4 mm. In our experiments, we did not observe a significant shift of the LPZ border from the day of the lesion onwards, so it is unlikely that retinal ‘stunning’ had a significant role. Last, estimates of long-term recovery might be exaggerated by a systematic underestimation, perhaps resulting from retinal ‘stunning’ of the extent of immediate reorganization (minutes to hours). Several studies<sup>1,7–10,32,33</sup> report immediate receptive field expansion after stimulus deprivation or retinal lesioning (but see ref. 11). Immediate changes extending more than 4.5 mm from the LPZ border have been reported<sup>10</sup> in cat area 17 after retinal detachment. Such changes<sup>9,10</sup> are commensurate with the extent of long-term reorganization reported elsewhere<sup>1,4,6</sup>, making it difficult to decipher what, if any, component of reorganization is long-term. Previous reports indicate that a significant fraction (about 10%) of parafoveal (2–5°) macaque V1 neurons receive excitatory inputs from 2° or further away<sup>28,34</sup>. It is then possible that the reported receptive field shifts reflect activity arising in the far reaches of the classical receptive field of cortical cells. This activity may initially be subthreshold, then rise above threshold after lesioning through relatively fast adaptive gain adjustments or downregulation of inhibition<sup>29,30</sup>. Retinal ‘stunning’ in the lesion surround might prevent this from manifesting immediately, causing it to masquerade later as ‘long-term’ cortical reorganization.

Our results also contrast with a recent report by Baker *et al.* of extensive reorganization in human visual areas, including area V1 (ref. 35). Those measurements were made in two adult human subjects who had been diagnosed with macular degeneration covering the fovea nearly 20 years earlier. In contrast, Sunness and Yantis found no significant plasticity in a human subject with a partial macular lesion diagnosed 2 years before measurement<sup>36</sup>, and this has been confirmed in a second subject with a relatively complete macular lesion (B.A.W., J. Liu and S. Nagadamari, unpublished observations). These human measurements, coupled with the present macaque data, indicate that large-scale cortical reorganization in adult V1 might not occur until at least several years after sensory deprivation.

Under the conditions of our experiment, intra-cortical horizontal connections are apparently not sufficient to allow V1 to regain anywhere near its previous functionality after retinal lesions, even though they might be sprouting new axonal boutons<sup>37</sup>. Should horizontal connections also prove ineffective elsewhere, this could support the notion that large-scale reorganization reported in other areas<sup>38,39</sup> (as well as in the visual system in early blindness<sup>40–42</sup>) might be mediated subcortically or through feedback projections<sup>43,44</sup>. In general, connections that span large distances do not easily form *de novo* in the adult central nervous system<sup>45,46</sup>, so plasticity is unlikely to be manifested in cases in which the formation of such connections is required. This is more likely to be true in areas with spatially restricted connectivity patterns and small, largely non-overlapping receptive fields (like V1). In contrast, areas with large, overlapping receptive fields and broad connectivity patterns might be able to reorganize effectively without requiring the formation of an extensive network of new connections (Fig. 5).

In summary, we have measured the spatial pattern of visually driven activity near the border of the lesion projection zone created in adult macaque V1 by a homonymous retinal lesion. Over 4–7 months we observed no significant change in the position of the BOLD-defined LPZ border. BOLD responses in the LPZ did not become visually driven, and this was confirmed by electrophysiological measurements of multi-unit action potentials. Taken together, these experiments indicate that little long-term reorganization

occurs in the LPZ and that neuronal responses in the LPZ do not recover to anything approaching their normal state. On the basis of these results a more critical examination of previous ideas about the degree and temporal course of area V1 reorganization after retinal lesions might be worthwhile.

Beyond the specific study of V1, we showed that fMRI could be used effectively to monitor cortical organization in the anaesthetized macaque preparation. The use of macaque fMRI in combination with experimental manipulations that can enhance plasticity is a powerful approach that promises to enhance our understanding of the processes of neural recovery and reorganization, and to provide a useful model for studying human recovery from stroke.

## METHODS

**Retinal lesions.** Using a photocoagulation laser (NIDEK GYC-2000; 532 nm) we induced homonymous retinal lesions in adult rhesus macaques under general anaesthesia (Fig. 1). The lesions required 10–77 overlapping small laser burns (power 310 mW, duration 0.2 s each) to obtain a single, round, well demarcated, homogeneous, extrafoveal scar with a diameter ranging from 600 to 1,200  $\mu\text{m}$  (Fig. 1). This destroyed the photoreceptor and bipolar cell layers as well as most of the ganglion cell layer (Fig. 1b). Histological confirmation was obtained in two of four animals (the remaining two are still alive). These animals were killed with pentobarbital under general anaesthesia, and the eyes were extracted and fixed by immersion in 3.7% formaldehyde prepared in 0.1 M sodium phosphate buffer. The eyes were later embedded and processed in Paraplast; horizontal sections 15–20- $\mu\text{m}$  thick were cut and stained with haematoxylin and eosin. Animal fundi were photographed in each experimental session, and we confirmed that all lesions remained stable throughout the course of the experiments.

**fMRI parameters.** We used multi-shot (eight-segment) gradient-recalled echo-planar imaging in a BIOSPEC 4.7 T/40 cm scanner (Bruker) with 50 mTm<sup>-1</sup> gradients. The acquisition parameters were TE = 20 ms, TR = 750 or 805 ms, flip angle = 40°. Either 15 or 17 axial slices were collected at 1 × 1 mm<sup>2</sup> in-plane resolution and 2-mm thickness. These were resampled accordingly and aligned to a full-brain anatomical scan acquired before lesioning by using an MDEFT sequence at 0.5 × 0.5 × 0.5 mm<sup>3</sup> resolution. ROIs were defined on the flattened version of each monkey's anatomical scan, and had an anatomical resolution of about 0.5 × 0.5 mm<sup>2</sup> along the cortical sheet.

**Animal preparation.** Four healthy adult *Macaca mulatta*, older than 4 years, were used for the experiments. All sessions were in full compliance with the guidelines of the European Community for the care and use of the laboratory animals (EUVD 86/609/EEC) and were approved by the local authorities (Regierungspräsidium). fMRI experiments were performed under general anaesthesia in accordance with previously published protocols<sup>16,19</sup>. The animal was intubated after induction with fentanyl (31  $\mu\text{g kg}^{-1}$ ), thio-pental (5 mg kg<sup>-1</sup>) and succinylcholine chloride (3 mg kg<sup>-1</sup>); anaesthesia was maintained with isoflurane (animals O97 and E01) or remifentanyl (0.5–2  $\mu\text{g kg}^{-1} \text{ min}^{-1}$ ; animals E02 and A01). Mivacurium chloride (5–7 mg kg<sup>-1</sup> h<sup>-1</sup>) was used after induction to ensure complete paralysis of the eye muscles. Lactate Ringer's with 2.5% glucose was infused at 10 ml kg<sup>-1</sup> h<sup>-1</sup> throughout the experiment. The temperature was maintained at 38–39°C. After achieving mydriasis with two drops of 1% cyclopentolate hydrochloride, each eye was fitted with hard contact lenses (Harte PMMA-Linsen; Wöhlk, Kiel, Germany) to bring it to focus on the stimulus plane (about 2 dioptres).

**Visual stimulation.** Stimuli were presented monocularly, always in the same eye for each animal, with an SVGA fibre-optic system (AVOTEC; Silent Vision) with a resolution of 640 pixels × 480 pixels and a 60-Hz frame rate.

In the first stimulation model (full field) we presented blocks of a 18.4° × 14.1° rotating polar checkerboard pattern (corresponding to 3.5-Hz visual modulation at 100% contrast) alternating with blocks of uniform background illumination every 30 or 32 s, depending on the animal, for a total of 12 cycles. For animals O97 and E01, 48-s blocks for four cycles were also used. This stimulus has been shown<sup>16,18</sup> to activate powerfully early visual areas. At times a 3.7° diameter dark circular occluder centred at 3.7° in the visual field opposite to the scotoma was also presented for control purposes.

In the second stimulation model (expanding rings), we used annuli 0.9° wide<sup>19</sup> whose outer radius expanded from either 0.3° or 0.9° to 6.9° in steps of 0.6° (12 or 11 annuli). The annular patterns were rotating checkerboards. Each annulus was presented for 6.0 or 6.5 s and the entire sequence of annuli was repeated 12 or 18 times per scan, depending on the animal.

**Analysis.** We used the mrVista software (Stanford, <http://white.stanford.edu/software/>) for data analysis<sup>19,47</sup>. We use the coherence of the fMRI series at the

fundamental stimulus frequency to measure the strength of the BOLD responses<sup>19,20</sup>. Our measure for coherence is

$$C = A(f_0) / \left( \sum_{f_0 - \Delta f/2}^{f_0 + \Delta f/2} A(f)^2 \right)^{1/2}$$

where  $f_0$  is the stimulus presentation frequency,  $A(f_0)$  the amplitude of the signal at that stimulation frequency, and  $\Delta f$  a range of frequencies around the fundamental. For the stimuli that we used,  $f_0$  corresponded to 12 or 18 cycles per scan and  $\Delta f$  was chosen to be a bandwidth of 12 cycles centred at  $f_0$ . For sessions with  $f_0$  equal to four cycles we set  $\Delta f$  from three to seven cycles. Note that the noise level of coherence depends on the chosen bandwidth so that, for  $\Delta f = 12$  cycles, coherence in the absence of visual modulation is expected to be  $1/(\Delta f + 1)^{0.5} = 0.28$ .

**Electrophysiology.** The animal (E02) was anaesthetized with remifentanyl and paralysed as described above for the fMRI experiments. Visual stimuli were presented monocularly through a high-resolution (1,024 pixels × 768 pixels) AVOTEC device. A linear array of 16 tungsten electrodes (impedance 200–800 k $\Omega$ ) at 1-mm intervals was placed across the border of the scotoma through a craniotomy that exposed the dura. The electrodes were lowered one by one under audio guidance and were advanced about 300  $\mu\text{m}$  from the point at which multi-unit activity was first audible. They were then allowed to settle for 15–20 min before manual receptive field (RF) mapping. RFs were mapped by using oriented bars (sizes 0.5° × 1°, 0.5° × 2°, 1° × 2° and 1° × 3°, with orientations 0°, 45°, 90° and 135°) first moved for a manual sweep of the central 12° of the monkey's left visual field, then flashed at 0.5–2.0 Hz over a range of promising visual field locations. Flashed and rotating square polar checkerboard stimuli (sizes 1° × 1°, 2° × 2° and 3° × 3°) were also used. The pattern of the sweep was standardized to ensure that we did not skip any receptive field locations, and care was taken to define the border of each multi-unit receptive field approximated by a rectangle. All the stimuli described were used for each experiment except the first, for which only the polars were used. At the end of RF mapping we advanced the electrode another 0.5–1.0 mm, waited for 15 min and repeated the process. In all penetrations, superficial and deep receptive fields were approximately commensurate and at the same location. Eye drift was about 1–2° during an experiment. With all electrodes lowered we recorded multi-unit activity under stimulation with the rotating full-field polar checkerboard alternating with uniform background illumination (every 10 s for experiments 2 and 3, and every 5 s for experiment 1). The signal was digitized at 20,833 Hz, band-pass filtered to lie between 312 and 10 kHz, and processed with Data Visualization and Analysis Software (Plexon) to select spikes with an amplitude greater than 3 s.d. above the mean. Multi-unit firing rate histograms (Fig. 4c) were calculated by binning the spike trains in 100-ms bins and averaging together all stimulus cycles (48 for each experiment). Latency was computed as the time after stimulus transition when the firing rate was more than 10% of the transient's peak for three consecutive 5-ms time bins.

Received 2 December 2004; accepted 16 February 2005.

- Gilbert, C. D. & Wiesel, T. N. Receptive field dynamics in adult primary visual cortex. *Nature* **356**, 150–152 (1992).
- Gilbert, C. D., Hirsch, J. A. & Wiesel, T. N. Lateral interactions in visual cortex. *Cold Spring Harb. Symp. Quant. Biol.* **55**, 663–677 (1990).
- Heinen, S. J. & Skavenski, A. A. Recovery of visual responses in foveal V1 neurons following bilateral foveal lesions in adult monkey. *Exp. Brain Res.* **83**, 670–674 (1991).
- Darian-Smith, C. & Gilbert, C. D. Topographic reorganization in the striate cortex of the adult cat and monkey is cortically mediated. *J. Neurosci.* **15**, 1631–1647 (1995).
- Gilbert, C. D. Adult cortical dynamics. *Physiol. Rev.* **78**, 467–485 (1998).
- Kaas, J. H. et al. Reorganization of retinotopic cortical maps in adult mammals after lesions of the retina. *Science* **248**, 229–231 (1990).
- Pettet, M. W. & Gilbert, C. D. Dynamic changes in receptive-field size in cat primary visual cortex. *Proc. Natl Acad. Sci. USA* **89**, 8366–8370 (1992).
- Chino, Y. M., Kaas, J. H., Smith, E. L., Langston, A. L. & Cheng, H. Rapid reorganization of cortical maps in adult cats following restricted deafferentation in retina. *Vision Res.* **32**, 789–796 (1992).
- Calford, M. B., Schmid, L. M. & Rosa, M. G. Monocular focal retinal lesions induce short-term topographic plasticity in adult cat visual cortex. *Proc. R. Soc. Lond. B* **266**, 499–507 (1999).
- Schmid, L. M., Rosa, M. G. & Calford, M. B. Retinal detachment induces massive immediate reorganization in visual cortex. *Neuroreport* **6**, 1349–1353 (1995).
- DeAngelis, G. C., Anzai, A., Ohzawa, I. & Freeman, R. D. Receptive field structure in the visual cortex: does selective stimulation induce plasticity? *Proc. Natl Acad. Sci. USA* **92**, 9682–9686 (1995).
- Murakami, I., Komatsu, H. & Kinoshita, M. Perceptual filling-in at the scotoma

- following a monocular retinal lesion in the monkey. *Vis. Neurosci.* **14**, 89–101 (1997).
13. Horton, J. C. & Hocking, D. R. Monocular core zones and binocular border strips in primate striate cortex revealed by the contrasting effects of enucleation, eyelid suture, and retinal laser lesions on cytochrome oxidase activity. *J. Neurosci.* **18**, 5433–5455 (1998).
  14. Rosa, M. G., Schmid, L. M. & Calford, M. B. Responsiveness of cat area 17 after monocular inactivation: limitation of topographic plasticity in adult cortex. *J. Physiol. (Lond.)* **482**, 589–608 (1995).
  15. Schmid, L. M., Rosa, M. G., Calford, M. B. & Ambler, J. S. Visuotopic reorganization in the primary visual cortex of adult cats following monocular and binocular retinal lesions. *Cerebral Cortex* **6**, 388–405 (1996).
  16. Logothetis, N. K., Guggenberger, H., Peled, S. & Pauls, J. Functional imaging of the monkey brain. *Nature Neurosci.* **2**, 555–562 (1999).
  17. Logothetis, N. K., Pauls, J., Augath, M., Trinath, T. & Oeltermann, A. Neurophysiological investigation of the basis of the fMRI signal. *Nature* **412**, 150–157 (2001).
  18. Tolias, A. S., Smirnakis, S. M., Augath, M. A., Trinath, T. & Logothetis, N. K. Motion processing in the macaque: revisited with functional magnetic resonance imaging. *J. Neurosci.* **21**, 8594–8601 (2001).
  19. Brewer, A. A., Press, W. A., Logothetis, N. K. & Wandell, B. A. Visual areas in macaque cortex measured using functional magnetic resonance imaging. *J. Neurosci.* **22**, 10416–10426 (2002).
  20. Engel, S. A., Glover, G. H. & Wandell, B. A. Retinotopic organization in human visual cortex and the spatial precision of functional MRI. *Cerebral Cortex* **7**, 181–192 (1997).
  21. Boynton, G. M., Engel, S. A., Glover, G. H. & Heeger, D. J. Linear systems analysis of functional magnetic resonance imaging in human V1. *J. Neurosci.* **16**, 4207–4221 (1996).
  22. Wandell, B. A. Computational neuroimaging of human visual cortex. *Annu. Rev. Neurosci.* **22**, 145–173 (1999).
  23. Sclar, G., Maunsell, J. H. R. & Lennie, P. Coding of image contrast in central visual pathways of the macaque monkey. *Vision Res.* **30**, 1–10 (1990).
  24. Lee, T. S., Mumford, D., Romero, R. & Lamme, A. F. The role of the primary visual cortex in higher level vision. *Vision Res.* **38**, 2429–2454 (1998).
  25. Rossi, A. F., Desimone, R. & Ungerleider, L. G. Contextual modulation in primary visual cortex of macaques. *J. Neurosci.* **21**, 1698–1709 (2001).
  26. Li, W., Thier, P. & Wehrhahn, C. Neuronal responses from beyond the classic receptive field in V1 of alert monkeys. *Exp. Brain Res.* **139**, 359–371 (2001).
  27. Rossi, A. F., Rittenhouse, C. D. & Paradiso, M. A. The representation of brightness in primary visual cortex. *Science* **273**, 1104–1107 (1996).
  28. Cavanaugh, J. R., Bair, W. & Movshon, J. A. Nature and interaction of signals from the receptive field center and surround in macaque V1 neurons. *J. Neurophysiol.* **88**, 2530–2546 (2002).
  29. Hendry, S. H. & Jones, E. G. Reduction in number of immunostained GABAergic neurons in deprived-eye dominance columns of monkey area 17. *Nature* **320**, 750–756 (1986).
  30. Rosier, A. M. *et al.* Effect of sensory deafferentiation on immunoreactivity of GABAergic cells and on GABA receptors in the adult cat visual cortex. *J. Comp. Neurol.* **359**, 476–489 (1995).
  31. Das, A. & Gilbert, C. D. Long-range horizontal connections and their role in cortical reorganization revealed by optical recording of cat primary visual cortex. *Nature* **375**, 780–784 (1995).
  32. Volchan, E. & Gilbert, C. D. Interocular transfer of receptive field expansion in cat visual cortex. *Vision Res.* **35**, 1–6 (1995).
  33. Fiorani, M. Jr, Rosa, M. G. P., Gattass, R. & Rocha-Miranda, C. E. Dynamic surrounds of receptive fields in primate striate cortex: A physiological basis for perceptual completion? *Proc. Natl Acad. Sci. USA* **89**, 8547–8551 (1992).
  34. Levitt, J. B. & Lund, J. S. The spatial extent over which neurons in macaque striate cortex pool visual signals. *Vis. Neurosci.* **19**, 439–452 (2002).
  35. Baker, C. I., Peli, E., Knouf, N. & Kanwisher, N. G. Reorganization of visual processing in macular degeneration. *J. Neurosci.* **25**, 614–618 (2005).
  36. Sunness, J. S., Liu, T. & Yantis, S. Retinotopic mapping of the visual cortex using functional magnetic resonance imaging in a patient with central scotomas from atrophic macular degeneration. *Ophthalmology* **111**, 1595–1598 (2004).
  37. Darian-Smith, C. & Gilbert, C. D. Axonal sprouting accompanies functional reorganization in adult cat striate cortex. *Nature* **368**, 737–740 (1994).
  38. Pons, T. P., Garraghty, P. E. & Mishkin, M. Lesion-induced plasticity in the second somatosensory cortex of adult macaques. *Proc. Natl Acad. Sci. USA* **85**, 5279–5281 (1988).
  39. Pons, T. P. *et al.* Massive cortical reorganization after sensory deafferentation in adult macaques. *Science* **252**, 1857–1860 (1991).
  40. Sadato, N., Okada, T., Honda, M. & Yonekura, Y. Critical period for cross-modal plasticity in blind humans: a functional MRI study. *Neuroimage* **16**, 389–400 (2002).
  41. Sadato, N. *et al.* Activation of the primary visual cortex by Braille reading in blind subjects. *Nature* **380**, 526–528 (1996).
  42. Cohen, L. G. *et al.* Functional relevance of cross-modal plasticity in blind humans. *Nature* **389**, 180–183 (1997).
  43. Angelucci, A., Levitt, J. B. & Lund, J. S. Anatomical origins of the classical receptive field and modulatory surround field of single neurons in macaque visual cortical area V1. *Prog. Brain Res.* **136**, 373–388 (2002).
  44. Angelucci, A. *et al.* Circuits for local and global signal integration in primary visual cortex. *J. Neurosci.* **22**, 8633–8646 (2002).
  45. Koeberle, P. D. & Bahr, M. Growth and guidance cues for regenerating axons: where have they gone? *J. Neurobiol.* **59**, 162–180 (2004).
  46. Fenrich, K. & Gordon, T. Canadian Association of Neuroscience review: axonal regeneration in the peripheral and central nervous systems—current issues and advances. *Can. J. Neurol. Sci.* **31**, 142–156 (2004).
  47. Wandell, B. A., Chial, S. & Backus, B. Visualization and measurement of the cortical surface. *J. Cogn. Neurosci.* **12**, 739–752 (2000).

**Supplementary Information** is linked to the online version of the paper at [www.nature.com/nature](http://www.nature.com/nature).

**Acknowledgements** We thank J. Horton and A. Wade for comments and suggestions, and C. Riedinger, R. Esaki, I. Kim, E. Lit, J. Pauls and J. Werner for technical help. We also thank L. Vaina, B. Rosen and the members of our laboratory for their advice and support. This work received support from a National Eye Institute (NEI) grant (S.M.S.), an NEI postdoctoral fellowship grant (A.S.T.), an NEI grant to B.A.W., a Howard Hughes Medical Institute Physician Postdoctoral Fellowship (S.M.S.), a National Institute of Neurological Disorders and Stroke grant (A.A.B.), a grant from the Max Planck Society and a Deutsche Forschungsgemeinschaft grant. S.M.S. is currently also affiliated with the Athinoula Martinos Center for Biomedical Imaging, Massachusetts General Hospital, CNY-Building 149, 13th Street, Charlestown, Massachusetts 02129-2000, USA.

**Author Contributions** S.M.S. took primary responsibility for the design and execution of all experiments, as well as for performing the analysis and preparing the manuscript. A.A.B. and M.C.S. contributed equally to this work. M.C.S. helped perform MRI experiments and analysis. A.A.B. helped with the analysis and familiarized us with the mrVISTA software. A.S.T. was intimately involved with all aspects of the work. M.A. provided technical support with the MRI experiments. A.S. provided help with the histological preparations and W.I. helped with retinal lesioning. B.A.W. and N.K.L. provided resources and acted in supervisory roles.

**Author Information** Reprints and permissions information is available at [npg.nature.com/reprintsandpermissions](http://npg.nature.com/reprintsandpermissions). The authors declare no competing financial interests. Correspondence and requests for materials should be addressed to S.M.S. ([smsmirnakis@partners.org](mailto:smsmirnakis@partners.org)).